LOW-TEMPERATURE PLASMA

Dynamics of Ionization Processes in High-Pressure Nitrogen, Air, and SF$_6$ during a Subnanosecond Breakdown Initiated by Runaway Electrons

V. F. Tarasenko, D. V. Beloplotov, and M. I. Lomaev

*Institute of High-Current Electronics, Siberian Branch, Russian Academy of Sciences,
Akademicheskii pr. 2/3, Tomsk, 634055 Russia*

National Research Tomsk State University, pr. Lenina. 36, Tomsk, 634050 Russia

e-mail: vft@loi.hcei.tsc.ru

Abstract—The dynamics of ionization processes in high-pressure nitrogen, air, and SF$_6$ during breakdown of a gap with a nonuniform distribution of the electric field by nanosecond high-voltage pulses was studied experimentally. Measurements of the amplitude and temporal characteristics of a diffuse discharge and its radiation with a subnanosecond time resolution have shown that, at any polarity of the electrode with a small curvature radius, breakdown of the gap occurs via two ionization waves, the first of which is initiated by runaway electrons. For a voltage pulse with an ~500-ps front, UV radiation from different zones of a diffuse discharge is measured with a subnanosecond time resolution. It is shown that the propagation velocity of the first ionization wave increases after its front has passed one-half of the gap, as well as when the pressure in the discharge chamber is reduced and/or when SF$_6$ is replaced with air or nitrogen. It is found that, at nitrogen pressures of 0.4 and 0.7 MPa and the positive polarity of the high-voltage electrode with a small curvature radius, the ionization wave forms with a larger (~30 ps) time delay with respect to applying the voltage pulse to the gap than at the negative polarity. The velocity of the second ionization wave propagating from the plane electrode is measured. In a discharge in nitrogen at a pressure of 0.7 MPa, this velocity is found to be ~10 cm/ns. It is shown that, as the nitrogen pressure increases to 0.7 MPa, the propagation velocity of the front of the first ionization wave at the positive polarity of the electrode with a small curvature radius becomes lower than that at the negative polarity.

1. INTRODUCTION

Studies of discharges in elevated-pressure gases have long attracted considerable interest [1–4]. This is associated with the complexity of the physical processes occurring in the gap and on the electrodes, as well as with a wide application area of such discharges in engineering and technology [4–6]. Recently, attention to studying atmospheric-pressure diffuse (volume) discharges initiated by runaway electrons (REs) (i.e., high-energy electrons generated in high-voltage gas discharges) has increased substantially (see [7] and references therein). The history of research in this field starts with the hypothesis of Wilson about the possibility of generating electrons with elevated energies in atmospheric discharges [8]. However, only 42 years after the pioneering work by Frankel et al. [9], generation of REs in a discharge in atmospheric-pressure helium was confirmed experimentally by detecting X-ray emission from the discharge gap. Diffuse discharges formed without applying an auxiliary preionization source in atmospheric-pressure helium [10]

and air [11] were described for the first time in the 1960s. In those works, it was reported about the detection of X-ray emission and the formation of a diffuse discharge. Later on, diffuse discharges formed in a nonuniform electric field without an auxiliary preionization source and accompanied by X-ray emission and RE generation were studied in many works (see, e.g., [7, 12–26] and references therein). However, the formation dynamics of such discharges still remains poorly studied; in particular, this concerns discharges formed in dense gases when a high-voltage pulse with a subnanosecond front is applied to the gap. This is related to the complexity of the processes occurring on the electrodes and in the gap, as well as to the high ionization rate at a high electric field strength near the electrode with a small curvature radius (~10^7 V/cm) and in the gap.

This work is aimed at studying the dynamics of ionization processes in nitrogen, air, and SF$_6$ during a diffuse breakdown initiated by REs in a nonuniform electric field generated by applying a high-voltage pulse

with a subnanosecond front. In our experiments, we used modern oscilloscopes with a picosecond time resolution, especially designed detectors intended to measure the discharge current and the current of the supershort avalanche electron beam (SAEB) behind the anode foil, and a photodiode with a subnanosecond time resolution. To interpret the experimental results, various processes affecting the development of ionization and radiation in the gap, as well as generation of REs and X-ray emission, are analyzed.

2. EXPERIMENTAL SETUP AND DIAGNOSTIC TECHNIQUES

Subnanosecond breakdowns in nitrogen, air, SF_6, and SF_6—nitrogen mixtures were studied using a setup consisting of a RADAN-220 generator [27] and a discharge chamber. The block diagram of the experimental setup and the schematic of the discharge chamber in which a plane electrode and a high-voltage electrode with a small curvature radius were mounted are shown in Fig. 1.

The voltage pulse from the generator was fed through transmission line *5* to electrode *7* with a small curvature radius. The voltage was measured using capacitive divider *6*, installed in front of the discharge gap. The full width at half-maximum of the voltage pulse at a matched load was ~2 ns, and the duration of the voltage pulse front in the transmission line was ~0.5 ns. The discharge current was measured using a current shunt *8*, made of low-inductance film resistors. High-voltage electrode *7*, made of a 100-μm-thick stainless-steel foil, had the shape of a 6-mm-diameter tube or a cone with a sharp vertex. Grounded plane grid electrode *9* was usually installed at a distance of 13 mm from the end of the high-voltage electrode. Behind the grid electrode, 50-μm-thick Al—Mg foil *10* was placed. The SAEB parameters were measure using collector *11*, installed behind foil *10*. Using lenses *3*, a twofold magnified image of the discharge plasma was produced on the screen with 1-mm-wide slit *2*, positioned in front of PD025 photodiode *1* with an LNS20 (Photek) cathode having an ~80-ps rise time of the transition characteristic. The screen with slit *2* and PD025 photodiode *1* were mounted on a movable platform, which allowed one to record radiation from different zones along the discharge gap with a spatial resolution of ~1 mm. For each zone, 100 radiation pulses and 100 corresponding voltage and current pulses were recorded, after which averaging was performed. Since the voltage and current waveforms did not depend on the position of the zone from which radiation was recorded, they were averaged over 1400 discharges.

Integral radiation from the gap was photographed with a Sony A100 digital camera. The discharge radiation spectra were recorded using an HR4000 (Ocean Optics B.V.) spectrometer with an operating spectral
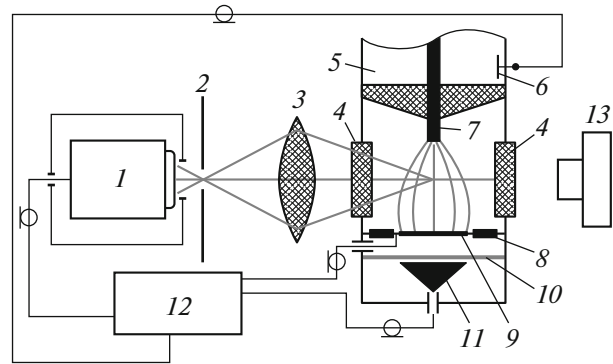
Fig. 1. Schematic of the experimental setup: (*1*) PD025 photodetector in a metal screen, (*2*) screen with a 1-mm-wide slit, (*3*) lens, (*4*) side window, (*5*) transmission line of the RADAN-220 generator, (*6*) capacitive voltage divider, (*7*) high-voltage electrode, (*8*) current shunt, (*9*) grounded grid electrode, (*10*) foil, (*11*) collector, (*12*) oscilloscope, and (*13*) Sony A100 photocamera or spectrometer.

range of $\Delta\lambda = 200-305$ nm and an EPP-2000C (Stellar-Net Inc.) spectrometer with an operating range of $\Delta\lambda = 200-850$ nm. Signals from the capacitive voltage divider, current shunt, collector, and photodiode were fed to a DPO70604 digital oscilloscope (6 GHz, 25 samples/ns). In some experiments, a DSA 72504D oscilloscope (25 GHz, 100 samples/ns) was used to measure the electric signals. The X-ray exposure dose was measured using Arrow—Tech, Inc (Model 138) dosimeters. The electron beam and X-ray emission were also fixed using an RF-3 film placed in a 120-μm-thick black paper envelope.

3. ANALYSIS OF THE EXPERIMENTAL CONDITIONS

3.1. Criterion for Electron Runaway in Gases

In this work, we have studied breakdown under RE generation conditions. Let us analyze these conditions for elevated-pressure gases by using results of [2, 8, 13—15, 28—30]. As was noted in the Introduction, the possibility of generating high-energy electrons in atmospheric discharges was predicted in [8]. The parameters of a stationary RE flow in weakly ionized plasma were calculated in [28] by solving the kinetic equation in a uniform electric field. According to [2, 13], where the approach used in [28] was further developed, the runaway condition (i.e., a monotonic increase in the energy of an electron in gas) is the requirement that the electric field strength be $E > E_{cr1}$, where the critical field strength E_{cr1} is determined by the maximum value of the decelerating force $E_{cr1} = F_{max}/e$ (where e is the elementary charge). Then,

according to [2], the expression for the critical field takes the form

$$E_{cr1} = \frac{4\pi e^3 ZN}{2.72I},\qquad(1)$$

or

$$\frac{E_{cr1}}{p} = 3\times10^3\,\frac{Z}{I[\text{eV}]}\,[\text{V/(cm Torr)}].$$

Here, p is the gas pressure at room temperature (293 K), Z is the number of electrons in an atom or a molecule of the neutral gas, N is the number density of neutral gas particles, and I is the average energy of inelastic losses. As a result, for helium in a uniform electric field, we obtain $E_{cr1}/p \approx 140$ V/(cm Torr), while for nitrogen, we have $E_{cr1}/p \approx 590$ V/(cm Torr). The criterion $E > E_{cr1}$ is local in a sense that the critical field E_{cr1} is determined only by the properties of neutral particles and the gas density at a given spatial point. When deriving the local criterion, generation low-energy electrons due to gas ionization was disregarded. According to this (local) criterion, electrons may pass into the runaway mode at relatively low electric fields; in particular, for atmospheric-pressure nitrogen, we have $E_{cr1} \approx 450$ kV/cm.

Multiplication of electrons was taken into account by Kozyrev et al. [29]; as a result, the critical field increased by about one order of magnitude (up to $E_{cr1}/p \approx 550$ and ≈ 4000 V/(cm Torr) for helium and nitrogen, respectively). According to the calculations presented in [29], a considerable fraction of electrons pass into the runaway mode at substantially stronger electric fields than it follows from [2, 13]. Thus, the critical field in atmospheric-pressure nitrogen was found to be $E_{cr1} \approx 3$ MV/cm. We note that the results of [29] were also cited in monograph [2]; however, no analysis of the applicability of two very different (by about one order of magnitude) criteria for electron runaway was given. In [2, 13, 28, 29], the critical field was found to be independent of the gas pressure and the gap length.

A nonlocal criterion for electron runaway was proposed by S.I. Yakovlenko and studied in detail in [14, 15]. It was shown that, when considering an ensemble of multiplying electrons, the concepts applied to a single electron can be inapplicable to all electrons. Accordingly, it is incorrect to consider that, at $E > E_{cr1}$, the average energy of electrons increases permanently with increasing distance x traveled by them. The matter is that electrons are multiplied exponentially (in an avalanche manner), whereas the energy gained by them in a uniform field increases only linearly with distance. Therefore, at sufficiently large distances, the average energy per one electron stops to grow with increasing x. This leads to the limitation of the average electron energy.

To determine the average electron energy, an equation taking into account the increase in the number of electrons was used in [14, 15]. It was shown that REs in gas begin to dominate when the interelectrode distance d becomes comparable with the characteristic multiplication length (the inverse first Townsend coefficient α_i^{-1}). Accordingly, the criterion determining the critical field strength E_{cr} has the form [14, 15]

$$\alpha_i(E_{cr}, p)d = 1.\qquad(2)$$

Since the dependence $\alpha_i(E)$ at a given p is nonmonotonic, criterion (2) can be met for two values of the field strength, $E_{cr} = E_{cr,up}$ and $E_{cr,down}$ (see Fig. 8 in [14]). It was shown that similar double-valued dependences also take place for different gases and for the reduced field strength $E_{cr}/p = U_{cr}/(pd)$, because the ratio E_{cr}/p, like U_{cr}, is a function of pd. The curve $U_{cr}(pd)$ separates the domain of efficient electron multiplication and the domain in which electrons leave the discharge gap without multiplication. It is universal for a given gas. According to the nonlocal criterion, the critical field for the runaway of most electrons is much larger than that following from local criterion (1) and nearly coincides with the critical field obtained in [29] for small values of the product $pd \sim 0.1$ cm Torr. For $pd \gg 0.1$ cm Torr, the critical field is much higher than that in [29]. The nonuniformity of the electric field in the discharge gap was taken into account in [30] by using a simplified model; however, no criterion for electron runaway was proposed.

It follows from the aforesaid that the critical field for electron runaway in a uniform electric field is rather high, which limits the number of REs generated during breakdown of a high-pressure gas. Therefore, in the first works on this subject, generation of X rays [9−11] and RE beams [12] in atmospheric-pressure gases was observed experimentally only when the curvature radius of at least one electrode was sufficiently small. This made it possible to produce a high local electric field and create conditions for electron runaway.

3.2. Generation Efficiency of Characteristic X Rays in Light Gases

In this section, we briefly describe the data from [31], where a high generation efficiency of characteristic radiation in nitrogen and oxygen was demonstrated. These data are important to explain the formation of diffuse discharges at the positive polarity of the electrode with a small curvature radius. Two main processes are responsible for the generation of X-ray emission in atmospheric-pressure air. First, this is electron bremsstrahlung on the nuclei of nitrogen and oxygen atoms. Second, this is ionization from the inner electron shells of these atoms (K shells), which leads to the generation of linear characteristic radiation due to cascade transitions of electrons from the upper energy levels into the formed vacancy. According to calculations [31], the efficiencies of bremsstrahlung and characteristic radiation depend on the atomic

number Z in opposite manners. The main process leading to absorption of soft X-ray emission in the gas volume is photoionization of atoms. For electrons with kinetic energies of several units of keV, energy losses are mainly caused by ionization from the K shells of nitrogen and oxygen. The intensity of bremsstrahlung of fast electrons on the atomic nuclei can be ignored. Calculations shows that, in centimeter-long discharge gaps filled with atmospheric-pressure air, REs excite characteristic radiation of nitrogen and oxygen atoms. According to [32], the energies $\hbar\omega_K$ of K-radiation photons of oxygen and nitrogen are 525 and 390 eV, respectively. The average ranges of such photons in atmospheric-pressure air (with allowance for the 80% partial concentration of nitrogen molecules) is ~4 mm. Absorption of K-radiation photons accompanied by knocking-out of secondary electrons with energies of ~120 eV occurs not far from the place of their generation, but quite far from the cascade of secondary electrons that appear due to impact ionization of air molecules by fast electrons. In the prebreakdown stage of the discharge, secondary electrons in the strong electric field can serve as centers of new electron avalanches; therefore, the above photoionization process of nitrogen by X-ray photons should lead to the formation of a diffuse discharge. This is confirmed by the formation of diffuse discharges in high-pressure gases when using an anode with a small curvature radius [7]. Characteristic X-ray emission, which, in contrast to the directed fast-electron flow, is almost isotropic, provides efficient gas photoionization both on the streamer head and near the region of the locally enhanced field at any voltage polarity of the electrode with a small curvature radius. The detection of intense characteristic radiation from a low-pressure discharge in xenon was reported in [33].

3.3. Ionization Wave in a Gap with a Nonuniform Electric Field

It is well known (see, e.g., [34–38]) that breakdown of a gas-filled gap with a nonuniform electric field occurs due to the formation of a streamer or an ionization wave (IW), which begins to propagate from the electrode with a small curvature radius. The propagation velocities of the streamer and the IW front depend on the pressure and sort of gas, the electric field strength, and the electrode design. For example, a streamer with a velocity of 0.6–1.2 mm/ns in atmospheric-pressure air and an even faster cathode-directed streamer were observed in [35]. In [36], a high-current negative streamer with a velocity of up to 20 cm/ns was reported. We suppose, however, that, in [36], the velocity of the front of the cathode-directed IW was actually measured.

According to [37], the velocity of the IW front was 13 cm/ns in atmospheric-pressure nitrogen and 5 cm/ns in SF$_6$. It also was established in [37] that the

velocity of the front of the cathode-directed IW was higher than that of the anode-directed IW.

In the present work, as in [37, 38], we studied the propagation of the IW front in the discharge gap. In contrast to the streamer, the IW has considerably larger transverse dimensions. Under these conditions, a diffuse discharge formed in the gap filled with nitrogen, air, or SF$_6$ at pressures of 0.1 MPa and higher. Discharges formed at elevated pressures due to preionization of the gap from an auxiliary source are usually called volume discharges [2, 3]. In this case, initial electrons are produced in the discharge gap, from which electron avalanches developed after applying a voltage pulse. For a sufficiently high density of initial electrons, the heads of the electron avalanches overlap before a transition of the avalanche into a streamer and a volume discharge forms in the discharge gap. The lifetime of the volume discharge depends on the experimental conditions. As the duration of the voltage pulse increases, it can contract and transform into a spark. High-pressure volume discharges are widely used to pump dense-gas lasers [39]. The properties of diffuse and volume discharges (the radiation spectrum, temperature, and the electron density) are close to one another. Therefore, these terms are often used as synonyms.
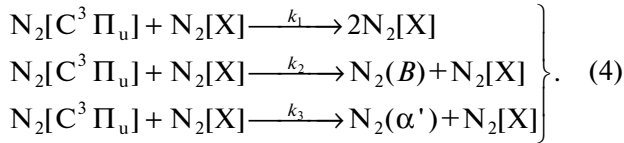
We note that a distinctive feature of a volume (diffuse) discharge initiated by an electron avalanche beam (VDIEAB) [40] is that no auxiliary preionization source is required for its formation and that the gap is filled with dense plasma due to the propagation of the IW front from the electrode with a small curvature radius. The development of breakdown in a nonuniform electric field will be considered in more detail below.

3.4. Effective Decay Time of the Second Positive System of Nitrogen at Elevated Pressures

To determine the propagation velocity of the IW front, we recorded UV radiation from different regions of the discharge gap. It is important that the deexcitation time of excited nitrogen molecules be sufficiently short. The spectral measurements performed in the present work and in [37, 38, 41] have shown that the intensity of the $C^3\Pi_u-B^3\Pi_g$ UV band of the second positive (2^+) system of nitrogen is the highest for VDIEABs in nitrogen, air, and SF$_6$–nitrogen mixtures. The effective lifetime of the $C^3\Pi_u$ state of a nitrogen molecule is determined by radiative and collision quenching and is described by the formula (see [41])

$$\tau_{\text{eff}} = \frac{\tau_{\text{sp}}}{1 + \tau_{\text{sp}}N_2[X](k_1 + k_2 + k_3)}$$
$$= \frac{\tau_{\text{sp}}}{1 + \tau_{\text{sp}}(k_1 + k_2 + k_3)(p/kT)}, \quad (3)$$

where τ_{sp} is the spontaneous lifetime; p is the gas pressure; T is the gas temperature; k is the Boltzmann constant; and k_1, k_2, and k_3 are the rates constants of reaction of the collision quenching of the $C^3\Pi_u$ (4) state,

$$\left.\begin{array}{l} N_2[C^3\Pi_u] + N_2[X] \xrightarrow{k_1} 2N_2[X] \\ N_2[C^3\Pi_u] + N_2[X] \xrightarrow{k_2} N_2(B) + N_2[X] \\ N_2[C^3\Pi_u] + N_2[X] \xrightarrow{k_3} N_2(\alpha') + N_2[X] \end{array}\right\}. \quad (4)$$

In formula (3) and reactions (4), $N_2[X]$, $N_2[C^3\Pi_u]$, $N_2(B)$, and $N_2(\alpha')$ are the populations of the corresponding states. The calculations were performed for the vales of the constants τ_{sp}, k_1, k_2, and k_3 taken from [42, 43]. The calculations show that, already at a nitrogen pressure of 2 atm, the effective decay time of the 2^+ system of nitrogen does not exceed 530 ps, whereas at a pressure of 7 atm, it is ~150 ps. Thus, UV radiation of the $C^3\Pi_u$−$B^3\Pi_g$ band of the 2^+ system of nitrogen can be used as a convenient spatiotemporal indicator of ionization processes during the RE-initiated breakdown of the discharge gap. The duration of the breakdown phase under our experimental conditions can be from a few tens of picoseconds to several hundred picoseconds, depending on the pressure. Therefore, to obtain more reliable information on the time behavior of the glow from different regions of the discharge gap, it is necessary to reduce the effective decay time of the 2^+ system of nitrogen by increasing the nitrogen pressure. We note that, in our experiments, the time resolution of the system for recording discharge radiation was 80 ps.

3.5. Relation between the Intensity of the 2^+ System of Nitrogen and the Development of Breakdown

Gas breakdown occurring in the discharge gap after applying a voltage pulse with a sufficiently large amplitude is accompanied by an increase in the degrees of excitation and ionization of the medium. Therefore, the dynamics of radiation in the initial stage of the discharge can provide initial information for the analysis of the breakdown process of the discharge gap. As was noted above, the VDIEAB emission spectrum in nitrogen and nitrogen-containing mixtures is dominated by radiation of the 2^+ system of nitrogen. In [38], the following equation was derived:

$$N_e(t)\left[\frac{dk_{exc}(t)}{dt} + k_i(t)[N_2]k_{exc}(t)\right] = \frac{\gamma}{[N_2]}\frac{d}{dt}\left[\frac{dI_D(t)}{dt} + \frac{I_D(t)}{\tau_{eff}}\right] \quad (5)$$

where $N_e(t)$ is the electron density, $k_{exc}(t)$ is the excitation rate constant, $k_i(t)$ is the ionization rate constant, $[N_2]$ is the density of nitrogen molecules, γ is a constant factor, $I_D(t)$ is the radiation intensity, and τ_{eff} is the effective lifetime of the $C^3\Pi_u$ state of a nitrogen molecule.

Equation (5) establishes the relationship (to within a constant factor γ) between the quantities that can be measured experimentally (on the right-hand side) and the quantities depending on the local value of the electric field strength $E(t)$ (on the left-hand side). Using this equation, one can determine the factors affecting the intensity and time behavior of radiation of the 2^+ system of nitrogen.

4. EXPERIMENTAL RESULTS

4.1. Formation of a Diffuse Discharge

Figure 2 shows photographs of a VDIEAB at (a) negative and (b) positive polarities of the voltage pulse, (c) a VDIEAB photograph in which one can see the spark leader approaching the cathode, and (d) a VDIEAB photograph in which one can see the formed spark channel. The results of the present study show that VDIEAB in a nonuniform electric field can form in different gases at elevated pressures for both polarities of the short-front voltage pulse. Within a relatively wide range of experimental conditions, at voltage pulse amplitudes of several hundreds kilovolts, the polarity of the electrode with a small curvature radius does not affect the VDIEAB formation in several-centimeter gaps. However, the formation of bright spots on the electrodes and the propagation velocity of the cathode- and anode-directed spark leaders, which lead to the contraction of the discharge, depend on the polarity of the electrode with a small curvature radius. The possibility of the formation of a diffuse discharge in atmospheric-pressure air when the negative polarity of the electrode with a small curvature radius is changed to the positive polarity was demonstrated for the first time in [44].

An increase in the gas pressure and/or voltage, a reduction in the gap length, and an increase in the pulse duration lead to VDIEAB contraction [41]. In the initial stage, a bright spot from which a spark leader then develops appears on the electrode. In Fig. 2, bright spots on the electrode with a small curvature radius that appear due to explosive electron emission [45] and the spark leader with a length of several millimeters are seen at both polarities of the voltage pulse. The appearance of bright spots on the plane electrode depends on its polarity and the gas pressure. At the negative electrode polarity, bright spots on the plane electrode are seen in a wider range of the experimental conditions. The time at which VDIEAB begins to contract can vary from pulse to pulse. Moreover, for the same experimental conditions, VDIEAB contraction can take place only in some pulses (rather than in each pulse) with the probability that varies from fractions of percent to 100% with decreasing gap length [41].

Our experiments have shown that, at the negative polarity of the electrode with a small curvature radius, the spark leader bridging the discharge gap grows from
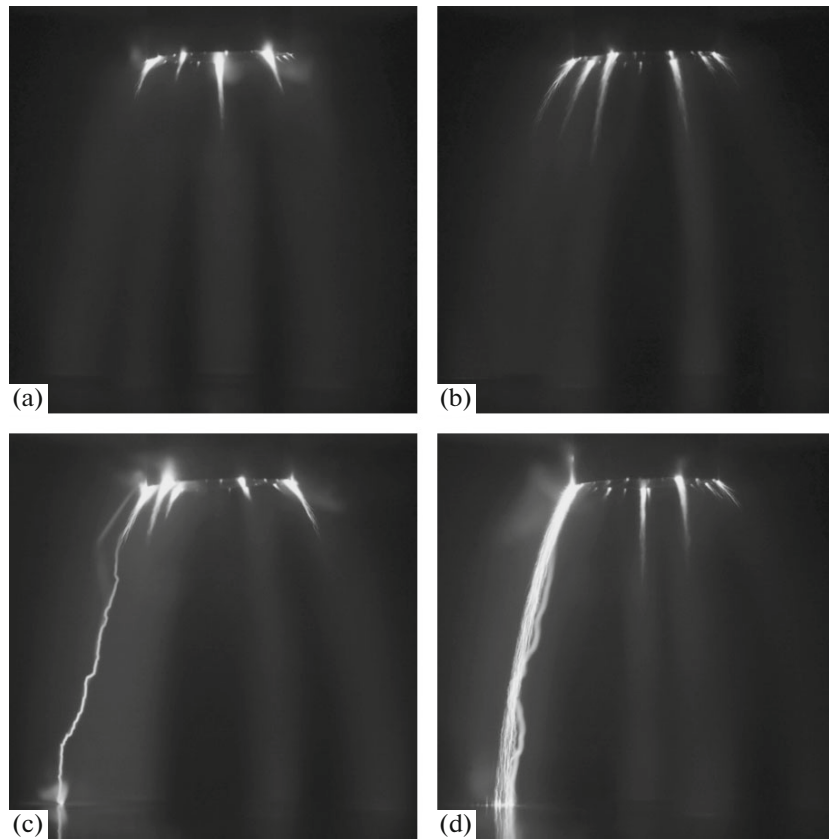
Fig. 2. Photographs of the discharge glow in nitrogen at a pressure of 0.3 MPa, a gap length of 13 mm, and the (a, c) negative and (b, d) positive polarity of the tubular electrode (on top). Variations in the discharge shape are caused by its instability from pulse to pulse.

the plane anode after the formation of a bright spot on it. Different stages of the development of the cathode-directed leader from the plane electrode were described in [46, 47]. Figure 2c shows a VDIEAB photograph in which one can see the anode spot and the cathode-directed spark leader approaching the cathode. In some pulses (Fig. 2d), against the background of a diffuse discharge, one can see the spark channel that formed after the discharge gap was bridged by the spark leader. The formation of spark leaders and the appearance of anode spots in experiments with the RADAN-220 generator at a voltage pulse amplitude of higher than 100 kV were studied in detail in [46—48], and those in experiments with the FPG-60 generator at voltage amplitudes of several tens of kilovolts were observed using a CCD camera in [49]. Since a two-electrode sharpening discharger was used in the RADAN-220 generator, it was impossible to synchronize the CCD camera and the beginning of breakdown of the discharge gap. The application of the FPG-60 generator and CCD camera made it possible to study the dynamics of breakdown in the gap in more detail [49].

For the positive polarity of the electrode with a small curvature radius, the spark leader bridging the gap usually propagates from the anode. However, in these experiments, in the entire pressure range under study and for both polarities of the voltage pulse, a diffuse discharge or a corona diffuse discharge (in SF_6 at elevated pressures) existed in a 13-mm-long gap over the first several nanoseconds and, after SAEB generation, spark leaders bridged the gap not earlier than in two nanoseconds after applying the voltage pulse. Accordingly, further we will present data on the radiation from the gap for the diffuse (volume) stage of the discharge, which corresponds to VDIEAB and during which the main contribution to the discharge radiation is given by the 2^+ system of nitrogen.

4.2. Amplitude and Temporal Characteristics of the Discharge Voltage and Current

Figure 3 shows typical waveforms of the discharge voltage for the negative polarity of the electrode with a small curvature radius and an air pressure of 0.2 MPa, as well as waveforms of the discharge and SAEB current pulses. The maximum of the voltage pulse in Fig. 3a nearly coincides with the time at which the SAEB is detected by the collector. At the same time, the waveform of the discharge current shows
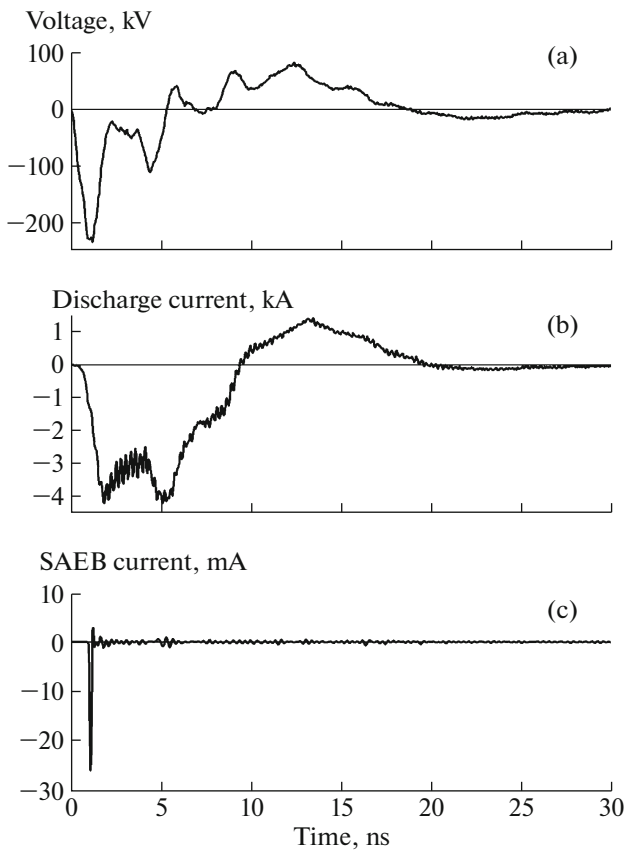
Voltage, kV

Discharge current, kA

SAEB current, mA

Time, ns

Fig. 3. Waveforms of the (a) voltage pulses, (b) discharge current, and (c) SAEB current (air at a pressure of 0.2 MPa).

a decrease in the growth rate of the current and some decrease in the current through the gap for large gaps and/or high pressures. Apparently, this is due to the escape of fast electrons onto the anode and the formation of a reversed electric field between the anode and positive ions remaining near it. The front of the current pulse through the gap has a complicated shape, which will be commented below. At the negative polarity of the generator, the SAEB was also detected by the exposure of the RF-3 film, which was placed in a black paper envelope behind the Al–Mg foil. To obtain a print of the beam current on the film, one pulse was sufficient. The highest blackening of the film was observed near the axis of the discharge gap.

The X-ray exposure dose at an air pressure of 0.1 MPa was 0.6 mR. This is the average value per pulse in a series of 50 pulses. To measure the X-ray exposure dose, the collector was removed, and the Al–Mg foil was replaced with a 20-μm-thick copper foil. The dosimeter was placed at a distance of 5 mm from the foil. The X-ray print was also recorded using a film protected by an additional filter absorbing electrons. Since the sensitivity of the RF-3 film to X-ray emission was much less than that to the electron beam,

it was necessary to produce more than one hundred pulses in order to obtain one print.

No SAEB was detected by the collector at the positive polarity of the voltage pulse, because REs moved toward the anode with a small curvature radius. For a 13-mm-long gap, even after 1000 pulses, no X-ray exposure dose was detected by the dosimeter. In this work, as in [50], X-ray emission at the positive polarity was detected only from the print on the film at a reduced gap length. To obtain one print, about 1000 pulses of the RADAN-220 generator were required.

Figure 4 shows voltage pulses of the positive and negative polarities across the discharge gap and waveforms of the discharge current recorded over the first 2 ns at nitrogen pressures of 0.4 and 0.7 MPa. For convenience of the comparison, the voltage and current values at the negative polarity of the voltage pulse were multiplied by −1. The voltage amplitude in discharges in nitrogen, air, and SF_6 increases with increasing pressure (Fig. 4a). For discharges in SF_6, VDIEAB forms at pressures lower than 0.2–0.25 MPa, whereas a diffuse corona discharge forms at higher pressures. In the waveform of the discharge current (Fig. 4b), one can distinguish three characteristic time intervals denoted as A, B, and C. Interval A corresponds to the capacitive current flowing until dense plasma appears in the discharge gap. This current decreases with decreasing dU/dt. The term "dense" means that the plasma electron density is sufficient to displace the electric field from the plasma. The increase in the current through the gap during the second time interval (B) corresponds to the appearance of the dynamic capacitive current, which arises after the formation of dense diffuse plasma at the electrode with a small curvature radius. The electron density in the IW plasma reaches 10^{13}–10^{14} cm^{-3} (see also [41, 51, 52]), due to which the electric field is displaced from the dense plasma region. The dynamic capacitive current increases due to the propagation of the IW front toward the plane electrode. The capacitance of the shrinking capacitor formed by the plane electrode and the dense plasma front increases as the plasma front approaches the plane electrode. This leads to an increase in the discharge current (including when dU/dt is reduced). In the third time interval (C), after bridging the gap by the dense plasma of the first IW, the current through the gap begins to grow due to an increase in the conduction current through the gap and the passage of the second IW. At the end of time interval B, the IW front reaches the plane electrode and the current through the gap is mainly determined by the conduction current. In time interval C, the second IW, as will be shown below, crosses the gap. During the propagation of the second IW the dynamic capacitive current between the front of the second IW and the electrode with a small curvature radius also contributes to the total discharge current. However, in

this case, additional preionization ahead of the front of the second IW is not required, because the electron density in the gap during a diffuse discharge in nitrogen already reaches ~10^{13} cm^{-3} [52]. It is also seen from Fig. 4b that the time delay between the beginning of the dynamic capacitive current (interval B) and the conduction current (interval C) increases with increasing gas pressure. One can also see the dependence on the voltage polarity. At the positive polarity, the dynamic capacitive current (interval B) and conduction current (interval C) are detected somewhat later than at the negative polarity. In the voltage pulses, the dependence on the polarity is traced in the time interval of 0.4—0.6 ns (Fig. 4a). It can be seen that, at the positive polarity, the voltage pulse amplitude is higher than at the negative polarity. The dependence of the beginning of the dynamic capacitive current (interval B), the conduction current (interval C), and the voltage pulse amplitude on the pressure and polarity will be discussed below.

4.3. UV Radiation from the Gap

UV radiation of the 2^+ system of nitrogen was detected in all gases under study (nitrogen, air, and SF$_6$). However, its intensity in SF$_6$ was low due to the low concentration of the nitrogen impurity; therefore, when studying the dynamics of radiation from the gap, we used SF$_6$ with a 2.5% nitrogen admixture. The maximum pressure of 0.7 MPa in these experiments was used when operating with nitrogen. In the experiments with air, SF$_6$, and the SF$_6$ + 2.5% N$_2$ mixture, the pressure did not exceed 0.3 MPa. Figure 5 shows waveforms of (a) the discharge voltage, (b) the discharge current, and (c) the radiation intensity from different zones along the gap, as well as the corresponding derivatives of the sum $dI_D(t)/dt + I_D(t)/\tau_{\text{eff}}$ (see Eq. (5)), in discharges in nitrogen at the negative voltage polarity and a pressure of 0.7 MPa. As was noted in Section 2, for each zone, 100 radiation pulses and 100 corresponding voltage and current pulses were recorded, after which averaging was performed. Similar time dependences of the radiation intensity, but only from the zones lying near the high-voltage and plane electrode, were obtained for other nitrogen pressures and for the SF$_6$ + 2.5% N$_2$ mixture. These dependences correspond to the dynamics of discharge radiation shown in Fig. 5c. The time delay between the appearance of the glow near the high-voltage electrode with a small curvature radius and that near the plane grounded electrode is typical of discharge formation in a nonuniform electric field (Fig. 5c). The time delay of the appearance of the glow near the electrode with a small curvature radius is almost independent of the sort and pressure of the gas. At the positive polarity and nitrogen pressures of 0.4 and 0.7 MPa, the glow near the anode with a small curvature radius appeared 30 ps later than at the negative polarity. The
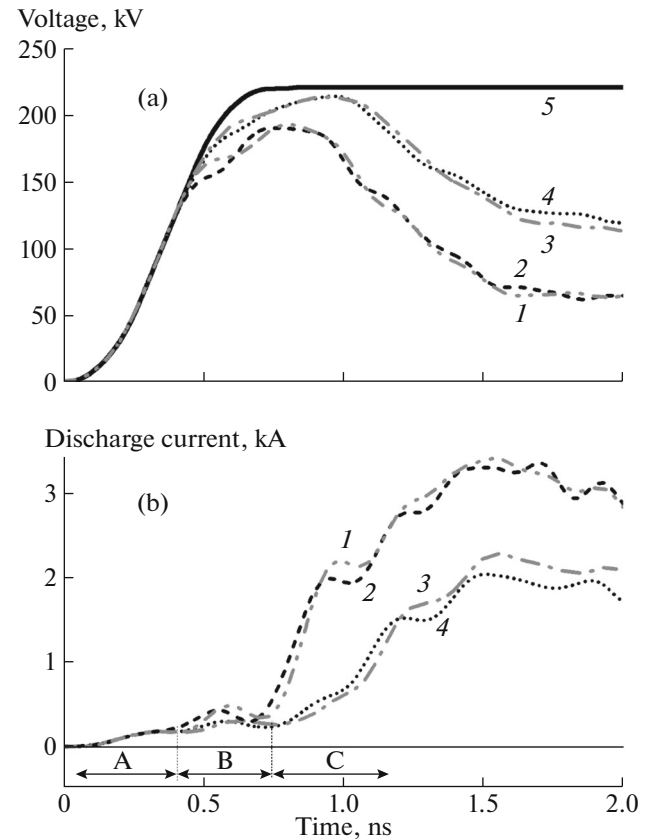

Fig. 4. Waveforms of the (a) voltage pulses and (b) discharge current in discharge in nitrogen at pressures of (1, 2) 0.4 and (3, 4) 0.7 MPa and at the (1, 3) positive and (2, 4) negative polarity of the electrode with a small curvature radius. The voltage and current values at the negative polarity are multiplied by −1. The time intervals indicated at the bottom of panel (b) correspond to (A) the capacitive current before the appearance of dense plasma in the discharge gap, (B) the dynamic capacitive current, and (C) the conduction current and the dynamic capacitive current.

time delay between the appearance of the glow near the electrode with a small curvature radius and that near the plane electrode depended on the pressure and polarity. The time delay of the appearance of the glow near the plane electrode was the shortest for nitrogen at the minimal pressure under study. For all gases, the time delay of the appearance of the glow near the plane electrode increased with increasing pressure. The curves shown in Fig. 5d and the waveforms of radiation pulses (Fig. 5c) allow one to analyze the left-hand side of Eq. (5). It can be seen in Fig. 5 that the time delay between applying the voltage pulse to the gap and the beginning of the passage of the conduction current and the voltage decay is about 1 ns. Within this time interval, the ionization processes develop in the gap, the degrees of excitation and ionization increase, and breakdown of the gap occurs. Therefore, the electron density $N_e(t)$ before parentheses on the left-hand side of Eq. (5) should increase monotoni-

Voltage, kV

Discharge current, kA

Intensity, arb. units

$d/dt[I_D(t)/\tau_{\mathrm{eff}} + dI_D(t)/dt]$, arb. units
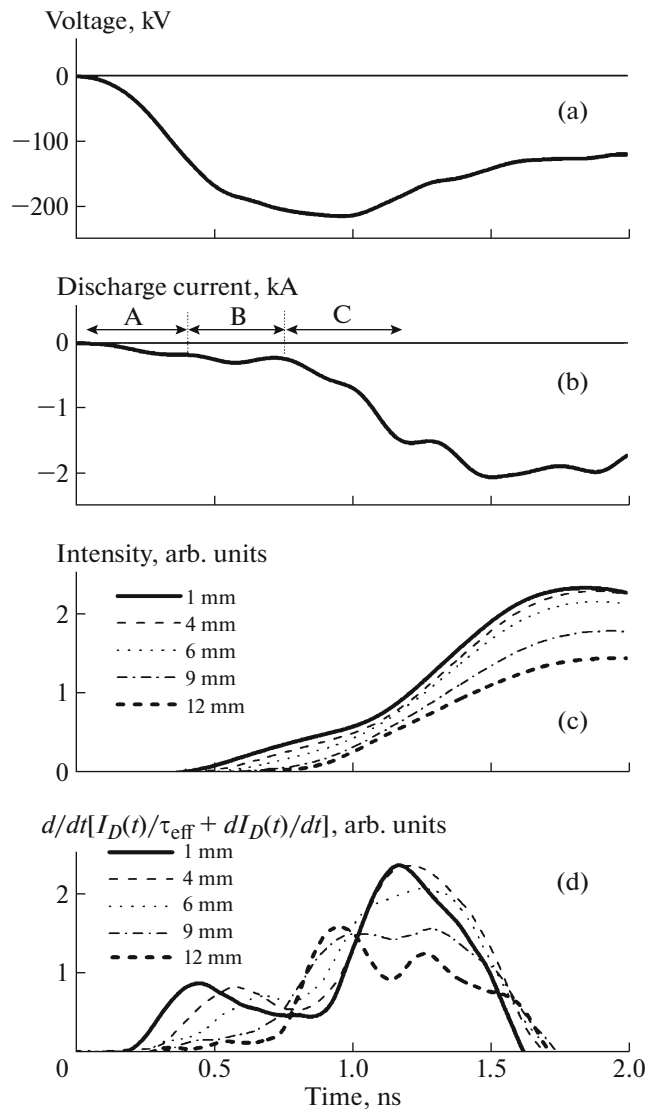

Time, ns

Fig. 5. Waveforms of the (a) voltage pulses, (b) discharge current, (c) radiation intensity from different zones along the gap, and (d) corresponding time derivatives of the sum $dI_D(t)/dt + I_D(t)/\tau_{\mathrm{eff}}$ (see Eq. (5)) in a discharge in nitrogen at a pressure of 0.7 MPa and the negative polarity of the electrode with a small curvature radius. The time intervals indicated in panel (b) correspond to (A) the capacitive current before the appearance of dense plasma in the discharge gap, (B) the dynamic capacitive current, and (C) the conduction current and the dynamic capacitive current.

cally in this time interval. However, it is seen from Fig. 5d that the right-hand side of Eq. (5) behaves nonmonotonically and has distinct maxima. For example, in the zone located at a distance of 1 mm from the electrode with a small curvature radius, the derivative of the sum $dI_D(t)/dt + I_D(t)/\tau_{\mathrm{eff}}$ begins to decrease after ~0.4 ns. In the zone located at a distance of 4 mm from the electrode with a small curvature radius, it begins to decrease after 0.6 ns. At the same

time, in the zone located at a distance of 12 mm, i.e., near the plane electrode, the derivative of the sum $dI_D(t)/dt + I_D(t)/\tau_{\mathrm{eff}}$ first increases slowly, but then a sharp jump takes place. Thus, the nonmonotonic behavior of the right-hand side of Eq. (5) can be related to the nonmonotonic time dependence of the expression $dk_{\mathrm{exc}}(t)/dt + k_i(t)[\mathrm{N_2}]k_{\mathrm{exc}}(t)$, which includes the excitation and ionization rate constants, $k_{\mathrm{exc}}(t)$ and $k_i(t)$, being functions of the reduced field. Under our experimental conditions, the average value of the reduced field, $E/p \approx 40$ V/(cm Torr), did not exceed the optimum value for the excitation of the 2^+ system of nitrogen, $(E/p)_{\mathrm{opt}} \approx 150-200$ V/(cm Torr), and the optimum value of E/p for gas ionization. Thus, the excitation and ionization rate constants should increase with increasing E/p (i.e., with increasing electric field at a constant pressure). Therefore, it may be concluded that, in the stage of breakdown, the observed decrease in the derivative of the sum $dI_D(t)/dt + I_D(t)/\tau_{\mathrm{eff}}$ in the zone located at a distance of 1 mm from the electrode with a small curvature radius after ~0.4 ns from the beginning of the voltage pulse can be due to a decrease in the electric field $E(t)$ in this zone. In the zones located at larger distances, such a decrease is observed at later time instants. The sharp jump of $dI_D(t)/dt + I_D(t)/\tau_{\mathrm{eff}}$ in the zone located at a distance of 12 mm from the electrode with a small curvature radius indicates that the field in this zone increases abruptly. The observed time dependences indicate that, under these conditions, breakdown of the gap occurs via the development of an IW. The spatiotemporal dependence of the right-hand side of Eq. (5) is presented most illustratively in Figs. 6 and 7. It is seen in these figures that the IW starts from the electrode with a small curvature radius and then propagates along the gap. After the IW passes about 2/3 of the gap filled with nitrogen at a pressure of 0.4 MPa (Fig. 6), the remaining part is broken down almost simultaneously or the IW velocity in this part of the gap increases abruptly. When the nitrogen pressure was 0.7 MPa (Fig. 7), the part of the gap in which breakdown occurred almost simultaneously decreased to ~1/4. Apparently, as the IW front propagates, the electric field in the part of the gap that is not yet broken is redistributed and becomes more uniform. When the reduced field in this part of the gap reaches a certain threshold value E/p, simultaneous ionization takes place. As the pressure increases, the threshold value of E/p is achieved at a shorter distance and simultaneous ionization occurs in the smaller part of the gap. After the first IW reaches the plane electrode, the second IW, propagating toward the electrode with a small curvature radius, forms. After the second IW arrives at the electrode with a small curvature radius, the breakdown stage terminates and the commutation stage begins. The commutation stage is accompanied by an abrupt increase in the conduction current, a decrease in the voltage (Figs. 4, 5a, 5b), and a sharp
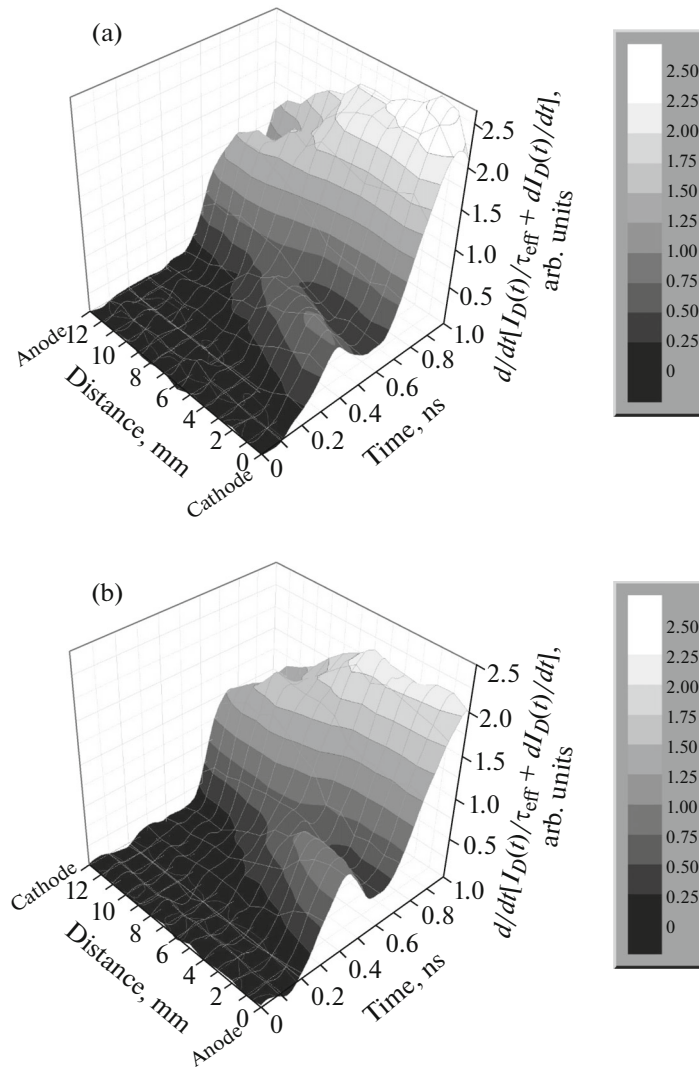
Fig. 6. Time derivative of the sum $dI_D(t)/dt + I_D(t)/\tau_{eff}$, which is proportional to the local electric field strength in the gap, as a function of time and the distance from the high-voltage electrode at the (a) negative and (b) positive polarity of this electrode (nitrogen at a pressure of 0.4 MPa).

increase in the radiation intensity (Fig. 5c). It should also be noted that, for the positive polarity, the decrease in the derivative of the sum $dI_D(t)/dt + I_D(t)/\tau_{eff}$ near the high-voltage electrode is observed at later times than for the negative polarity. It may be concluded that, for the positive polarity, the IW forms somewhat later with respect to applying the voltage pulse to the gap than for the negative polarity. This conclusion is confirmed by the waveforms of the current pulse shown in Fig. 4b (time interval B). One can see that, at the positive polarity, the dynamic capacitive current caused by the passage of the IW through the gap is detected somewhat later than at the negative polarity.

Figure 8 shows the time delay between the appearance of the glow near the electrode with the small curvature radius and that near the plane electrode versus gas pressure for pure nitrogen and the $SF_6 + 2.5\%\ N_2$ mixture, obtained in two series of experiments with different generator voltages. The time at which the signal level reached 5% of the maximum signal value from a given zone was taken as the beginning of the radiation glow from this zone. The signal-to-noise ratio was larger than 2. During the breakdown of the $SF_6 + 2.5\%\ N_2$ mixture, the time delay of the beginning of the glow near the plane electrode was much longer than that explained by the fact that SF_6 is a heavier electronegative gas having a higher breakdown voltage. As was noted above, the time delay of the appearance of the glow near the plane electrode is affected by the polarity of the high-voltage electrode. The time delay is smaller for the positive polarity (Fig. 8a) at nitrogen and SF_6 pressures of 0.3 MPa and lower. This indicates the higher IW propagation veloc-
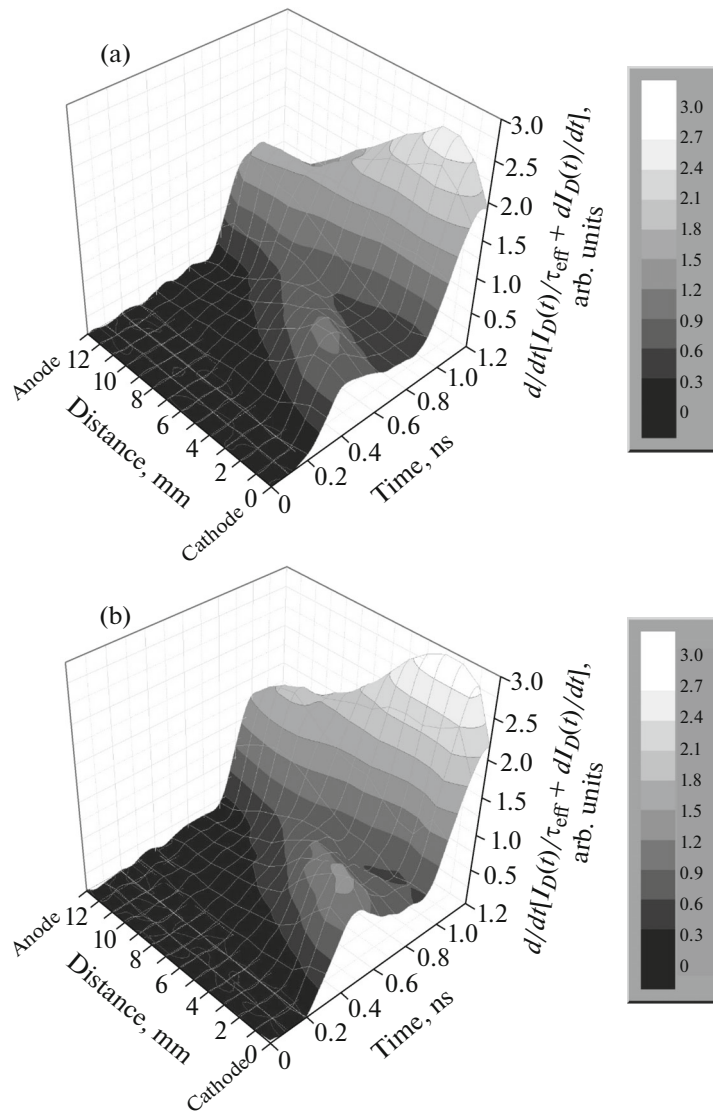
Fig. 7. The same as in Fig. 6, but for a nitrogen pressure of 0.7 MPa.

ity at the positive polarity of the voltage pulse, which agrees with the results obtained for the positive streamer [35] and IW [37, 38] in a discharge in atmospheric-pressure air. However, at a nitrogen pressure of 0.7 MPa, the situation was different; namely, at the negative polarity of the voltage pulse, the time delay of the appearance of the glow near the plane electrode was shorter and, accordingly, the propagation velocity of the IW front was higher.

5. DISCUSSION

Using the data obtained in this work and known from the literature (see [7] and references therein) on the formation of a VDIEAB, the following dynamics of the main ionization processes in the gap has been established. Breakdown of an elevated-pressure gas at

subnanosecond and nanosecond durations of the voltage pulse front in a point−plane gap begins with the field emission from the point cathode [53] or self-ionization of gas molecules near the point anode [54]. The observed time delay of ~30 ps in the formation of the IW at the positive polarity of the voltage pulse is apparently due to the difference in the mechanisms of electron emission (field emission and autoionization). Since the critical electric fields for these mechanisms of electron emission are higher than the critical field for electron runaway [2, 13−15, 28, 29], a fraction of electrons pass into the runaway mode near the point electrode. It is these fast electrons that produce initial gas ionization near the point electrode. Electrons avalanches with overlapping heads develop from the initial electrons appearing due to gas ionization by REs. As a result, dense diffuse plasma forms near the elec-

trode with a small curvature radius at both polarities of the voltage pulse. The electron and ion densities in this plasma are sufficient to displace the electric field from it, as is the case in the streamer head [1, 3]. The front of the dense diffuse plasma propagates toward the plane electrode due to an increase in the electric field ahead of this front and gas preionization by both REs and X-ray and VUV emission. In other words, in the beginning of breakdown, a dense plasma cloud with transverse dimensions much larger than those of the streamer propagates from the electrode with a small curvature radius to the plane electrode. Due to their large mass, ions remain almost at rest, while the propagation of the IW front toward the plane electrode is provided by electron multiplication in a narrow layer with an enhanced electric field. However, the mechanisms for gas preionization ahead of the IW front at the positive and negative polarities of the electrode with a small curvature radius are different.

For the negative polarity of the point electrode, a region with an excess negative charge forms at the boundary of the dense plasma, as is in the head of an electron avalanche or a streamer. However, there is a significant difference in the transverse dimensions of the electron avalanche plasma and the IW plasma formed during the VDIEAB development. Due to this difference, the electric field ahead of the IW front is much higher. Accordingly, the electron density in the IW is higher than in the avalanche and the IW front propagates toward the anode with a substantially higher velocity. A fraction of electrons at the boundary of the region with an excess negative charge are accelerated due to both the applied electric field and the negative charge of the electron cloud at the boundary of the dense plasma. As the IW front propagates in the region with an enhanced electric field, conditions are created for the generation of REs due to polarization self-acceleration. According to this mechanism, a fraction of electrons on the polarized streamer front propagating with a high velocity in the electric field can be accelerated to high energies. This mechanism of particle acceleration at the streamer front was proposed by Askar'yan [55]. During polarization self-acceleration, the number of REs moving from the boundary of the dense plasma (from the IW front) increases in the course of IW propagation, which eventually leads to an increase in the SAEB amplitude behind the foil anode. The electron energy in this case also increases [56]. Thus, the propagation of the front of the first IW is provided by both REs, which produce gas preionization, and the high electric field ahead of the IW front. New electron avalanches, the heads of which also overlap, develop from the initial electrons generated due to gas ionization by REs. Dense plasma forms at the highest rate near the IW front, where the electric field is the most enhanced.

Before the appearance of dense plasma, the current through the gap is almost capacitive and is caused by the charging of the discharge gap capacitance. For a
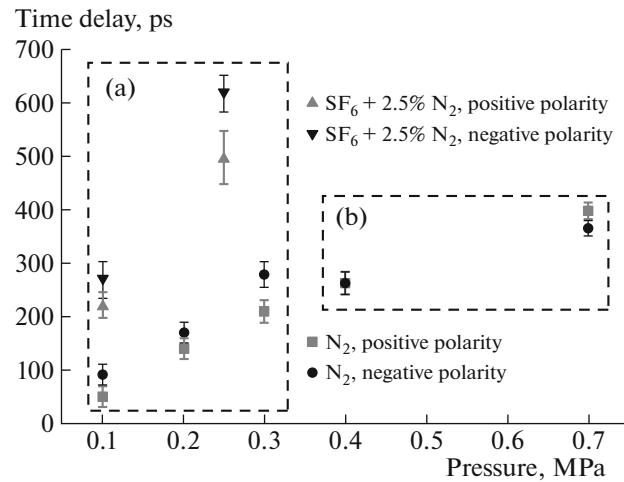

Fig. 8. Time delay between the appearance of the glow near the high-voltage electrode and that near the plane electrode vs. gas pressure at the negative and positive polarities of the voltage pulse for discharges in pure nitrogen and the $SF_6 + 2.5\% N_2$ mixture: (a) the first series of experiments and (b) the second series of experiments with a reduced generator voltage.

voltage pulse with a subnanosecond front, this current can reach several hundred amperes, depending on the cathode design and the voltage pulse amplitude [7, 26]. After the formation of dense plasma near the cathode with a small curvature radius, the current flowing through the gap begins to rapidly increase and, in several tens to several hundred picoseconds reaches values from a few hundred amperes to several kiloamperes. The increase in the current is caused by the charging of the shrinking capacitor formed between the front of the dense plasma and the anode [57]. The main mechanism of electron emission from the cathode becomes explosive electron emission [45]. This mechanism is confirmed by the appearance of bright spots on the cathode in a time on the order of 100 ps and the erosion of the sharp cathode edges [58].

After the propagation of the first IW, the gap becomes bridged by the dense plasma. It was established experimentally that the front of the first IW accelerated in the course of its propagation (Figs. 6, 7). It was also found that, at the positive polarity of the high-voltage electrode with a small curvature radius and nitrogen pressures of 0.4 and 0.7 MPa, the first IW formed with a somewhat larger time delay with respect to applying the voltage pulse than at the negative polarity. When the electron beam reaches the anode, the total current through the gap decreases, but it increases again after REs go to the anode. Measurements of the plasma glow from different regions of the discharge gap and the subsequent analysis of Eq. (5) show that, after the first IW has passed from the electrode with a small curvature radius to the plane electrode, the second IW begins to propagate from the

plane electrode to the electrode with a small curvature radius (Figs. 6, 7). The current flowing through the gap during the propagation of the second IW is also provided by explosive electron emission from the cathode with a small curvature radius.

At the positive polarity of the high-voltage electrode with a small curvature radius, there are mainly positive ions and a region with an excess positive charge on the cathode side near the boundary of the dense plasma. Electrons near the boundary of this region are accelerated due to both the applied electric field and the positive charge of the ion cloud at the boundary of the dense plasma. As was noted above, the first electrons near the point anode appear due to autoionization before the plasma formation [54]. Some of these electrons can pass into the runaway mode and generate X-ray emission after arriving at the anode. However, strong electric fields required for autoionization are present only in a narrow region near the anode, due to which the voltage drop across this region turns out to be insufficient for electron acceleration and the energy of REs arriving at the anode does not exceed several keV. Therefore, it is rather difficult to detect X-ray emission at the positive polarity of the electrode with a small curvature radius. In this work, we succeeded to detect X-ray emission only from the print on the X-ray film recorded over a large number of pulses at gap lengths not exceeding fractions of a millimeter. We consider that, in this case, X-ray bremsstrahlung from both the gas and the anode was detected, the intensity of anode emission being very low. At the positive polarity, the energy of REs was low, because they escaped into the dense plasma of the IW and onto the anode. The intensity of X-ray bremsstrahlung generated in collisions of electrons with light atoms is also low, and the energy of photons of K-shell characteristic X-ray emission in nitrogen and oxygen is lower than 600 eV [31].

However, characteristic X rays are emitted into the full solid angle, including toward the cathode, thereby preionizing the gap. As a result, electron avalanches, the heads of which overlap, continue to develop from initial electrons produced by X-ray emission from the anode and the IW front propagates toward the cathode. A fraction of electrons ahead of the IW front gain energies from a few keV to several tens of keV and X-ray emission is generated in their interaction with the gas. It is well known that the efficiency of bremsstrahlung generation decreases with decreasing electron energy and atomic number of the target material. However, the efficiency of generation of characteristic X-ray emission in light gases at electron energies from a few keV to several tens of keV is much higher than the efficiency of bremsstrahlung generation [31]. At the positive polarity of the electrode with a small curvature radius, the gap is also bridged by the IW and not only REs, but also X-ray emission, play an important role in the generation of initial electrons. In the case of an anode with a small curvature radius, the passage of

the current through the gap during the propagation of the IW is provided by both the charging of the shrinking capacitor formed between the front of the dense plasma and the plane cathode and the conduction current flowing through the dense plasma. However, when the dense plasma arrives at the cathode, the shrinking capacitor is short-circuited and a need arises in an efficient mechanism of electron generation from the cathode. We consider that, after the cathode-directed IW arrives at the plane cathode, electrons are supplied in the gap mainly due to explosive electron emission from the cathode. Explosive-emission centers (bright spots) are clearly seen in the photographs of the discharge at high gas pressures (see, e.g., Fig. 2d). At the positive polarity of the electrode with a small curvature radius, in a wide range of experimental conditions (excluding at pressures higher than 0.4 MPa), the increase in the conduction current during the propagation of the second IW occurs with a larger time delay than that at the negative polarity (see Figs. 6–8). As a result, the polarity effect in different gases is inverted [59].

At both polarities of the electrode with a small curvature radius, the main role in the formation of a volume diffuse discharge is played by REs and most REs are generated due to an increase in the electric field during the formation of electron avalanches. This is why we call this type of discharge a volume discharge initiated by an electron avalanche beam (VDIEAB). In our previous publications [7, 58], we called this type of discharge a runaway electron preionized diffuse discharge (REP DD).

A high-pressure volume discharge in a uniform electric field forms due to gas preionization by various ionizing sources (an electron beam, X rays, or VUV and UV photons) [2]. In a nonuniform electric field at nanosecond voltage pulses, the gap is preionized by REs generated near the electrodes and in the gap, as well as by bremsstrahlung and characteristic X-ray emission. The formation of a diffuse discharge under these conditions is determined by the presence of an internal preionization source.

6. CONCLUSIONS

Complex studies of the dynamics of the ionization processes in high-pressure nitrogen, air, and SF_6 during the breakdown of a gap with a nonuniform distribution of the electric field by nanosecond high-voltage pulses have been performed. The dynamics of the main ionization processes in high-pressure nitrogen, air, and SF_6 during a subnanosecond breakdown initiated by REs is examined.

The measurements of the amplitude and temporal characteristics of the discharge and its radiation with a subnanosecond time resolution confirm the results obtained earlier in [37, 38]. In particular, it is shown that, at both polarities of the electrode with a small

curvature radius, breakdown of the gap occurs via the IW initiated by REs and X-ray emission. The IW propagation velocity increases with decreasing pressure and when the SF_6 gas is replaced with lighter gases (air or nitrogen) and reaches about 15 cm/ns in nitrogen at a pressure of 0.1 MPa at the positive polarity of the electrode with a small curvature radius.

It is shown that, after the passage of the first IW, the second IW begins to propagate from the plane electrode. The velocity of the second IW in nitrogen at a pressure of 0.7 MPa and the negative polarity of the electrode with a small curvature radius is about 10 cm/ns. It is established that, as the nitrogen pressure increases to 0.7 MPa, the propagation velocity of the front of the first IW at the negative polarity is higher than that at the positive polarity. At nitrogen pressures of 0.4 and 0.7 MPa and the positive polarity of the high-voltage electrode with a small curvature radius, the first IW forms with a larger time delay (~30 ps) with respect to applying the voltage pulse to the gap than at the negative polarity. It is shown that the velocity of the first IW increases after its front has passed one-half of the gap. As the nitrogen pressure increases, the increase in the IW velocity is observed at larger distances from the electrode with a small curvature radius.

ACKNOWLEDGMENTS

REFERENCES

1. H. Raether, *Electron Avalanches and Breakdown in Gases* (Butterworths, London, 1964).
2. Yu. D. Korolev and G. A. Mesyats, *Physics of Pulsed Gas Breakdown* (Nauka, Moscow, 1991) [in Russian].
3. Yu. P. Raizer, *Gas Discharge Physics* (Nauka, Moscow, 1987; Springer-Verlag, Berlin, 1991).
4. *Encyclopedia of Low-Temperature Plasma,* Vol. VIII-1: *Chemistry of Low-Temperature Plasma,* Ed. by Yu. A. Lebedev, N. A. Plate, and V. E. Fortov (Yanus-K, Moscow, 2005) [in Russian].
5. *Low Temperature Plasma: Fundamentals, Technologies, and Techniques,* Ed. by R. Hippler, H. Kersten, M. Schmidt, and K. H. Schoenbach (Wiley−VCH Verlag, Weinheim, 2008).
6. *Low Temperature Plasma Technology,* Ed. by P. K. Chu and X. P. Lu (CRC, Boca Raton, 2014).
7. *Runaway Electrons Preionized Diffuse Discharges,* Ed. by V. F. Tarasenko (Nova Science, New York, 2014).
8. C. T. R. Wilson, Proc. Cambridge Philos. Soc. **22**, 534 (1924).
9. S. Frankel, V. Highland, T. Sloan, O. Van Dyck, and W. Wales, Nucl. Instrum. Methods Phys. Res. **44**, 345 (1966).
10. R. C. Noggle, E. P. Krider, and J. R. Wayland, J. Appl. Phys. **39**, 4746 (1968).
11. L. V. Tarasova and L. N. Khudyakova, Sov. Phys. Tech. Phys. **14**, 1148 (1969).
12. L. V. Tarasova, L. N. Khudyakova, T. V. Loiko, and V. A. Tsukerman, Sov. Phys. Tech. Phys. **19**, 351 (1975).
13. L. P. Babich, T. V. Loiko, and V. A. Tsukerman, Sov. Phys. Usp. **36**, 592 (1990).
14. V. F. Tarasenko and S. I. Yakovlenko, Phys. Usp. **47**, 887 (2004).
15. *Proceedings of the Prokhorov General Physics Institute, Russian Academy of Sciences,* Ed. by S. I. Yakovlenko (Nauka, Moscow, 2007), Vol. 63 [in Russian].
16. J. E. Chaparro, W. Justis, H. G. Krompholz, L. L. Hatfield, and A. Neuber, IEEE Trans. Plasma Sci. **36**, 2505 (2008).
17. A. G. Rep'ev and P. B. Repin, Tech. Phys. **53**, 73 (2008).
18. V. I. Karelin and A. A. Tren'kin, Tech. Phys. Lett. **35**, 407 (2009).
19. L. P. Babich and T. V. Loiko, Plasma Phys. Rep. **36**, 263 (2010).
20. T. Shao, C. Zhang, Z. Niu, P. Yan, V. F. Tarasenko, E. Kh. Baksht, A. G. Burachenko, and Yu. V. Shut'ko, Appl. Phys. Lett. **98**, 021503 (2011).
21. V. F. Tarasenko, Plasma Phys. Rep. **37**, 409 (2011).
22. D. Levko, Ya. E. Krasik, and V. F. Tarasenko, Int. Rev. Phys. **6**, 165 (2012).
23. T. Shao, V. F. Tarasenko, W. Yang, D. V. Beloplotov, Ch. Zhang, M. I. Lomaev, P. Yan, and D. A. Sorokin, Plasma Sources Sci. Technol. **23**, 054018 (2014).
24. S. Yatom, D. Levko, V. Vekselman, J. Z. Gleizer, V. Vekselman, and Y. E. Krasik, Appl. Phys. Lett. **100**, 024101 (2012).
25. G. A. Mesyats, M. I. Yalandin, A. G. Reutova, K. A. Sharypov, V. G. Shpak, and S. A. Shunailov, Plasma Phys. Rep. **38**, 29 (2012).
26. I. D. Kostyrya, D. V. Rybka, and V. F. Tarasenko, Instrum. Exp. Tech. **55**, 72 (2012).
27. F. Ya. Zagulov, A. S. Kotov, V. G. Shpak, Ya. Ya. Yurike, and M. I. Yalandin, Prib. Tekh. Exp., No. 2, 146 (1989).
28. A. V. Gurevich, Sov. Phys. JETP **12**, 904 (1960).
29. A. V. Kozyrev, Yu. D. Korolev, G. A. Mesyats, and Yu. N. Novoselov, *VI All-Union Conference on Physics of Low-Temperature Plasmas, Leningrad, 1983,* Book of Abstracts, p. 228.
30. A. M. Boichenko, A. G. Burachenko, I. D. Kostyrya, V. F. Tarasenko, and A. N. Tkachev, Tech. Phys. **56**, 1202 (2011).
31. A. V. Kozyrev, V. F. Tarasenko, E. Kh. Baksht, and Yu. V. Shut'ko, Tech. Phys. Lett. **37**, 1054 (2011).
32. *Handbook of Physical Quantities,* Ed. by I. S. Grigoriev and E. Z. Meilikhov (Energoatomizdat, Moscow, 1991; CRC, Boca Raton, 1997).
33. V. O. Ponomarenko and G. N. Tolmachev, Tech. Phys. Lett. **38**, 747 (2012).
34. S. M. Starikovskaia, N. B. Anikin, S. V. Pancheshnyi, D. V. Zatsepin, and A. Y. Starikovskii, Plasma Sources Sci. Technol. **10**, 344 (2001).

35. D. Wang, M. Jikuya, S. Yoshida, S. Katsuki, and H. Akiyama, IEEE Trans. Plasma Sci. **35**, 1098 (2007).

36. L. M. Vasilyak, S. P. Vetchinin, and D. N. Polyakov, Tech. Phys. Lett. **25**, 749 (1999).

37. D. V. Beloplotov, M. I. Lomaev, D. A. Sorokin, and V. F. Tarasenko, Opt. Atmos. Okeana **27**, 316 (2014).

38. M. I. Lomaev, D. V. Beloplotov, V. F. Tarasenko, and D. A. Sorokin, IEEE Trans. Dielect. Elect. Insul. **22**, 1833 (2015).

39. G. A. Mesyats, V. V. Osipov, and V. F. Tarasenko, *Pulsed Gas Lasers* (Nauka, Moscow, 1991; SPIE Press, Washington, 1995).

40. V. F. Tarasenko, V. M. Orlovskii, and S. A. Shunailov, Izv. Vyssh. Uchebn. Zaved., Fizika, No. 3, 94 (2003).

41. M. I. Lomaev, D. V. Rybka, D. A. Sorokin, V. F. Tarasenko, and K. Yu. Krivonogova, Opt. Spectrosc. **107**, 33 (2009).

42. J. Makuchowski and L. Pokora, Opt. Appl. **23**, 113 (1993).

43. I. A. Kossyi, A. Yu. Kostinsky, A. A. Matveyev, and V. P. Silakov, Plasma Sources Sci. Technol. **1**, 207 (1992).

44. I. D. Kostyrya and V. F. Tarasenko, Izv. Vyssh. Uchebn. Zaved., Fizika, No. 12, 85 (2004).

45. G. A. Mesyats and D. I. Proskurovsky, *Pulsed Electrical Discharge in Vacuum* (Nauka, Novosibirsk, 1984; Springer-Verlag, Berlin, 1989).

46. V. F. Tarasenko, E. Kh. Baksht, A. G. Burachenko, M. I. Lomaev, D. A. Sorokin, and Yu. V. Shut'ko, Tech. Phys. **55**, 904 (2010).

47. Ch. Zhang, V. F. Tarasenko, T. Shao, D. V. Beloplotov, M. I. Lomaev, R. Wang, D. A. Sorokin, and P. Yan, Phys. Plasmas **22**, 033511 (2015).

48. T. Shao, V. F. Tarasenko, Ch. Zhang, M. I. Lomaev, D. A. Sorokin, P. Yan, A. V. Kozyrev, and E. Kh. Baksht, J. Appl. Phys. **111**, 023304 (2012).

49. V. F. Tarasenko, E. Kh. Baksht, A. G. Burachenko, and M. V. Erofeev, High Voltage Eng. **39**, 2105 (2013).

50. T. Shao, Ch. Zhang, Z. Niu, P. Yan, V. F. Tarasenko, E. Kh. Bakst, I. D. Kostyrya, and Yu. V. Shut'ko, J. Appl. Phys. **109**, 083306 (2011).

51. S. Yatom and Y. E. Krasik, J. Phys. D **47**, 215202 (2014).

52. D. A. Sorokin, M. I. Lomaev, T. I. Banokina, and V. F. Tarasenko, Tech. Phys. **59**, 1119 (2014).

53. G. N. Fursey, *Field Emission in Vacuum Microelectronics* (Plenum, New York, 2005).

54. E. W. Muller, J. A. Panitz, and S. B. McLane, Rev. Sci. Instrum. **39**, 83 (1968).

55. G. A. Askar'yan, Tr. FIAN **66**, 66 (1973).

56. V. F. Tarasenko, E. Kh. Baksht, A. G. Burachenko, I. D. Kostyrya, and D. V. Rybka, Plasma Phys. Rep. **39**, 592 (2013).

57. V. F. Tarasenko, E. Kh. Baksht, A. G. Burachenko, I. D. Kostyrya, M. I. Lomaev, and D. V. Rybka, Tech. Phys. **55**, 210 (2010).

58. E. Kh. Baksht, A. G. Burachenko, I. D. Kostyrya, M. I. Lomaev, D. V. Rybka, M. A. Shulepov, and V. F. Tarasenko, J. Phys. D **42**, 185201 (2009).

59. T. Shao, V. F. Tarasenko, Ch. Zhang, D. V. Beloplotov, W. Yang, M. I. Lomaev, Zh. Zhou, D. A. Sorokin, and P. Yan, Phys. Lett. A **378**, 1828 (2014).

Translated by L. Mosina